DESIGN AND SIMULATION OF A LOW-COST BIOSENSOR FOR POINT-OF-CARE DIAGNOSE DEVICES

By Gonzalo Álvarez Viar

Academic Tutorship: Juan José Vaquero

Tutorship: Jose Javier Serrano Olmedo

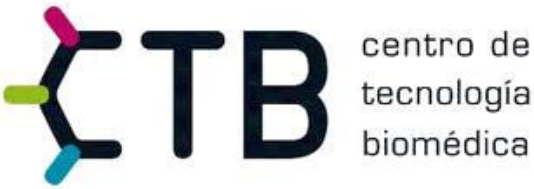

I want to express my gratitude to

Cristina Sánchez López de Pablo,

Luis Armando Carvajal,

José Javier Serrano Olmedo

and all my colleagues in the

Center of Biomedical Technology (UPM).

I have learnt so much from all of you.

INDEX

CHAPTER 1. INTRODUCTION

MOTIVATION

Some diseases are no longer among us in developed countries. Moreover, some of them are or were extinct like smallpox (thanks to Edward Jenner who discovered a vaccine for this illness in 1798). However, the chasm between rich and poor has only widened, due to deprivation and war. This situation has produced a global relapse of some of these diseases, like tuberculosis, inside developing countries. Diagnose has been proven to be a limiting step regarding medical treatment, present as a determinant factor for quick patient healing. The conditions are extremely challenging for a help-less person to access any of the fairy simple medical treatments available for TB (There are several well known antibiotics which are effective against this infection[1]). In addition there is a need for high sensitivity diagnostic tools, able to detect the presence of this infection even in its latent state (the effective number of particles of interest is lower) Although both diagnosis and treatment for the disease are fairly simple, medical centres use to be inexistent, far away and/or overwhelmed in disaster or isolated zones. Further more, it is paramount to provide a reliable identification of the bacterial family causing the infection as specific antibiotics have to be administered to fight each of them.

Point Of Care Testing (POCT) is often accomplished through the use of transportable, portable, and handheld instruments (e.g., blood glucose meter, nerve conduction study device) and test kits (e.g., CRP, HBA1C, Homocystein, HIV salivary assay, etc.). Devices like this are a robust approach of effective healthcare delivery within places with these conditions. In addition to this very urgent issue, a significant reduction of the patient turnaround time at hospitals around the world can be achieved inexpensively, provided the low-cost batch fabrication and operation of the devices. The standardization of miniaturized technology within hospitals would also reduce human labour costs. Additionally, the scale reduction of the whole diagnosis procedure implies also a reduction in the amount of reagents, waste generation and energy consumption. The reasons are countless to participate in such a laudable project, regardless the negligible personal profit involved.

The principal aim of the work is to help in the development of a low-cost biosensor capable of providing a reliable diagnosis to inexpert users. Rather than being a precise measurement instrument like mass spectrometers, this biosensor should be able to qualitatively detect and distinguish between the most relevant families of the bacteria causing *mycobacterium tuberculosis* in human fluids. Other approaches pursue outstanding sensitivity relying on expensive materials and microfabrication processes. Despite other requisites,

low-cost imposes certain criteria regarding materials, systems, fabrication techniques and user interfaces to be included in the device.

This work is part of the PLADEBACT project (Platform for Detection of Bacteria in Human Fluids). It carries on with the already finished intramural project Nanophor. Several research groups are collaborating within this platform:

COORDINATOR RESEARCH GROUP: GIB-US

PRINCIPAL INVESTIGATOR: Javier Reina

OTHER GROUPS:

Group: GBT-UPM PI: José Javier Serrano

Group: GBIO-CNM PI: Jordi Aguiló

CLINICAL GROUPS:

Institution: Unit of Nephrology – University Hospital Virgen Macarena (UN-UHVM, Sevilla)

PI: Nuria Aresté Fosalba (Mercedes Salgueira)

EXTERNAL GROUPS:

Institution/ Company: Centro de Investigación y Desarrollo Tecnológico de la Industria Electro-Electrónica e Informática de Colombia (CIDEI)

PI: Vicente García

Institution/ Company: Experimental Microbiology Laboratory, Institute of Tropical Medicine Alexander von Humboldt, Universidad Peruana Cayetano Heredia: EMLIMT-UPCH.

PI: Palmira Ventosilla (José Chauca)

The aim of my group's work in the long term is at developing a prototype of quartz balance for the detection of Koch bacillus. Based on several simulations performed with COMSOL program, monophasic circuitry modelling was used to simulate the electrical behaviour of the system looking forward to its probing. To do so, a data acquisition system was also theorized and later prototyped in LabView. The next step is to build a simple prototype with a real crystal in order to exhaustively characterize the optimal configurations of media, stimulation regimes, and data acquisition strategies. The availability of

the prototype can shed light on the real problems regarding requisites, biofunctinalization, noise filtering, performance and operation sequences. Other groups like the one from UPCH are focused on the biofunctionalization of the device and the identification of potential biological targets to be detected. Nevertheless techniques related to electrode biofunctionalization and characterization of the biosensor will also be addressed. The bacteria detection itself is out of scope of this half-course work, but different approaches towards bacterial detection techniques will be covered.

In general terms, the working principles of the biosensor rely on the change in frequency spectrum response of a thickness shear oscillating quartz crystal due to the adsorption of specific biomolecular species present in the analyte at low concentrations on the surface of a gold electrode.

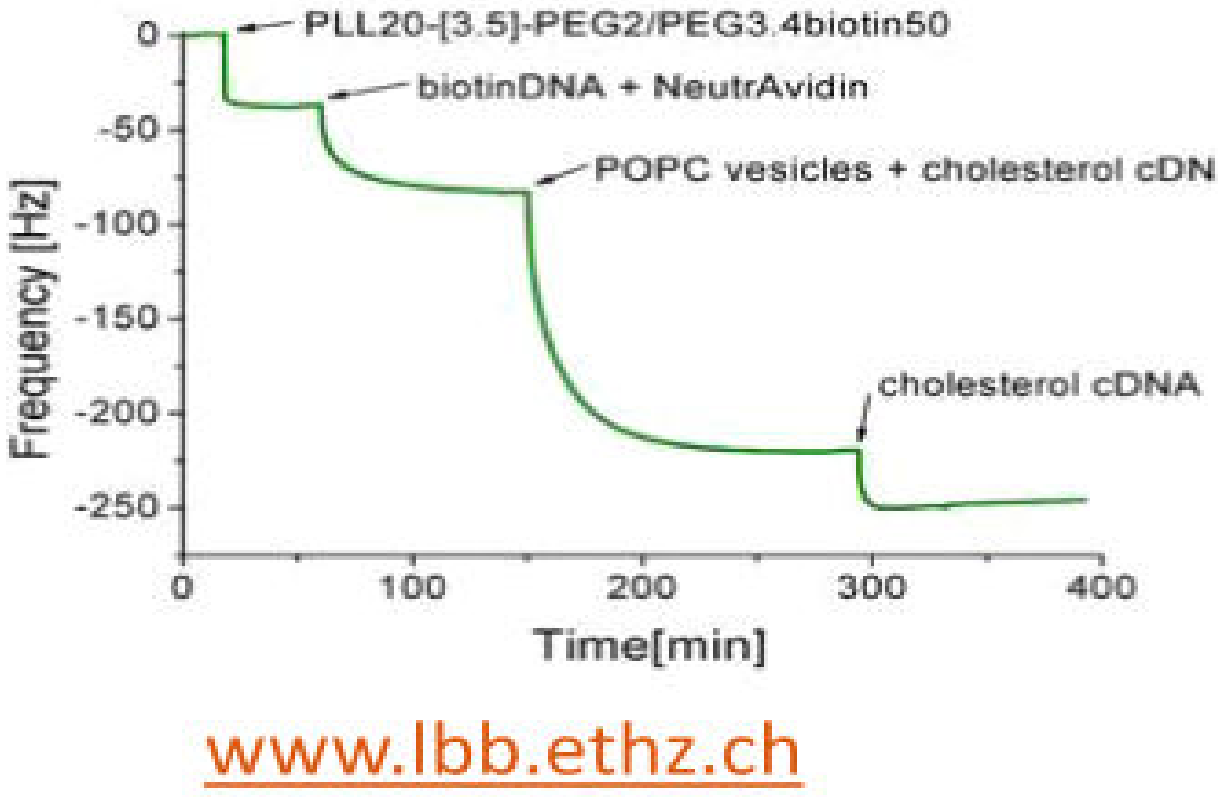

Fig.1.

Displacements in resonant frequency of the QCM depending on the composition of the analyte.

BRIEF HISTORY OF THE QUARTZ MICROBALANCE

-Piezoelectricity

In 1881 the Curie brothers (Pierre and Jacques) observed for the first time in documented science the phenomenon of piezoelectricity, on which the biosensor is based. It is true that long time ago, in 1672 sodium and potassium mixed tartarate ($KNaC_4H_4O_6 \cdot 4H_2O$), commonly known as Seignette's salt or Rochelle's salt (also piezoelectric) was discovered by Pierre Seignette working for Rochelle pharmaceutics. The phenomenon consists in the creation of an electron current inside matter due to a deformation suffered by crystalline networks and vice versa. Despite the fact that only 21 of the 32 crystalline structures known do show the asymmetry needed for piezoelectricity, 31 of them showed piezoelectric behaviour to a greater or lesser extent. If pressure is exerted along the polar axis, polarization is increased depending on the rate of variation in the deformation associated to that pressure.

One of its first uses was as an electric lighter (another piece slammed the quartz crystal generating a voltaic arc that could light something else). During First World War the piezoelectric phenomenon was widely used in sonar, clocks, and electronics. It was quickly included in the design of audio systems like microphones. In 1949 Mason[2] used it to study the viscoelasticity of certain fluids. Its use is widespread as oscillator in informatics to synchronize the operation of the CPU and its peripherals, due to its unmatched stability in frequency, purity in phase, and outstanding invariability under significant changes in temperature and moisture. Nowadays high-precision systems like GPS or space shuttles use atomic oscillators. However, this approach is much more expensive and requires cutting-edge technologies so quartz is still in use for many household applications.

Piezoelectricity is everywhere in our technology today. The piezoelectric capability of exerting and recording extremely low deformations make them really useful for micro-manipulation systems like digital microscope, scanning tip microscopy, high resolution ink printers and high-precision injectors for internal combustion engines. In general, another step was taken towards the manipulation of the micro-scale, setting up some of the bases for nanotechnology.

-State of the Art

Techniques involving a Quartz Micro Balance (QCM) commonly use a small disk of quartz (from 5 to 20 mm of diameter) with a thickness ranging

from some sets of tens of microns to 1mm approximately. Its resonant frequency depends on its piezoelectric properties, its dimensions, the type of cut and the mass of the metal electrodes deposited on its surfaces. A variable potential can be applied to the electrodes producing a variable deformation of the crystal. The ability to measure the resonant frequency *in situ* at the same time metal is deposited on the surface allows for precise determination of the crystals resonance reaching ppm. Resonant frequencies of this systems range from some kHz to sets of tens of MHz.

Many specialized approaches using this core technology have arisen. Its usefulness in many fields of science was been proven worldwide specially in electrochemistry. Within this field, electrochemical QCM technology shed light onto the reaction mechanisms involved in many phenomena like: Li intercalation, electrodeposition, corrosion studies, electropolymerization, ion/solvent adsorption and transport binding events. It was the advance in electrochemistry what made flourish QCM technologies the most.

Advances in microfabrication allow for high resolution designs and high precision cuts. This is the key for Multichannel QCM[3], in which different measurements can be carried on simultaneously on a single quartz crystal. For that means, small electrodes have to be precisely deposited over the quartz at specific resonance points. This involves cutting-edge microfabrication and micromanipulation technologies.

There is a global tendency to couple QCM cells to other systems like spectrometers[4], AFMs Atomic Force Microscopes and SECMs (Scanning Electrochemical Microscopes). By using combined technologies, several parameters can be estimated at the same time for a sample, resulting in a synergistic complement of calculations for high-level analysis. A great example is the development of a quartz crystal microbalance with dissipation coupled to on-chip MALDI-ToF (Matrix-Assisted Laser Desorption/Ionization Time-of-Flight) mass spectrometry as a tool for characterising proteinaceous conditioning films on functionalised surfaces.

By taking advantage of this technological breakthroughs, some groups have been able to study the dynamics of several biomacromolecular interactions like lipid-protein, protein-protein and membrane based biosensors[5]. The core technology here is the use of dissipation monitoring QCM (QCM-D). This allows for viscosity measurements and conditions control. It has been used to characterize supported lipid bilayers[5] (SLBs) which are an interesting platform to develop new biosensing technologies. They mimic the actual cell membrane and are supported by the substrate, in this case, the QCM electrode. New insights in molecular biology are coming up thanks to this technique.

CHAPTER 2. MATERIALS AND METHODS

MATERIALS

The materials used for the development of the experiments were as follows:

- Electronics laboratory circuitry
- PC (COMPAQ presario)
- Data acquisition card (National Instruments USB X SERIES)
- Digital oscilloscope (Tektronix TDS 2024B)
- Analog oscilloscope (Tektronix TDS 524A)
- Electronic components (R, C, L)
- Electric welder + Sn + Cu connection board
- Function generator (TTi TG5011)
- Multimeter
- LabView
- COMSOL (simulations by Luis Armando Carvajal)
- SketchUp
- https://www.circuitlab.com/

All this equipment was facilitated by the Bioinstumentation and Nanomedicine Laboratory (UPM) under the supervision of Javier Serrano Olmedo and with the close collaboration of Luis Armando Carvajal. There exist pictures of the equipment used listed within the annex.

THE QUARTZ CRYSTAL RESONATOR

The type of crystal used for the biosensing application is an AT cut quartz slab. The reason why this particular orientation for the slab is used resides in its vibration mode. A standing wave is set up in the crystal blank by the reflection at both major surfaces of traversal waves travelling in the thickness direction. The major mechanical displacement is in the plane of the crystal at right angles to the direction of propagation. At resonance an odd number of half wave lengths are contained in the thickness plane of the crystal blank. Therefore the thickness is the primary frequency determining dimension.

Here is an illustration of the vibration mode:

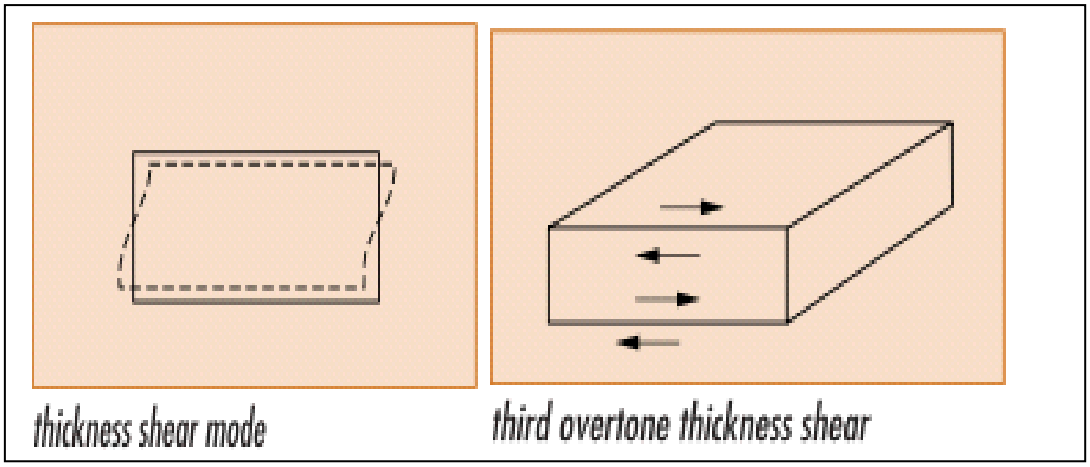

Fig.2.
Graphic representation of the thickness shear mode and its third overtone.

For each vibration mode there is certain angle of the cut that optimizes temperature stability of the resonant frequency. Here there are two images showing possible cuts with respect to the original crystal and variation in frequency due to temperature changes in AT cuts at different angles from 35º15':

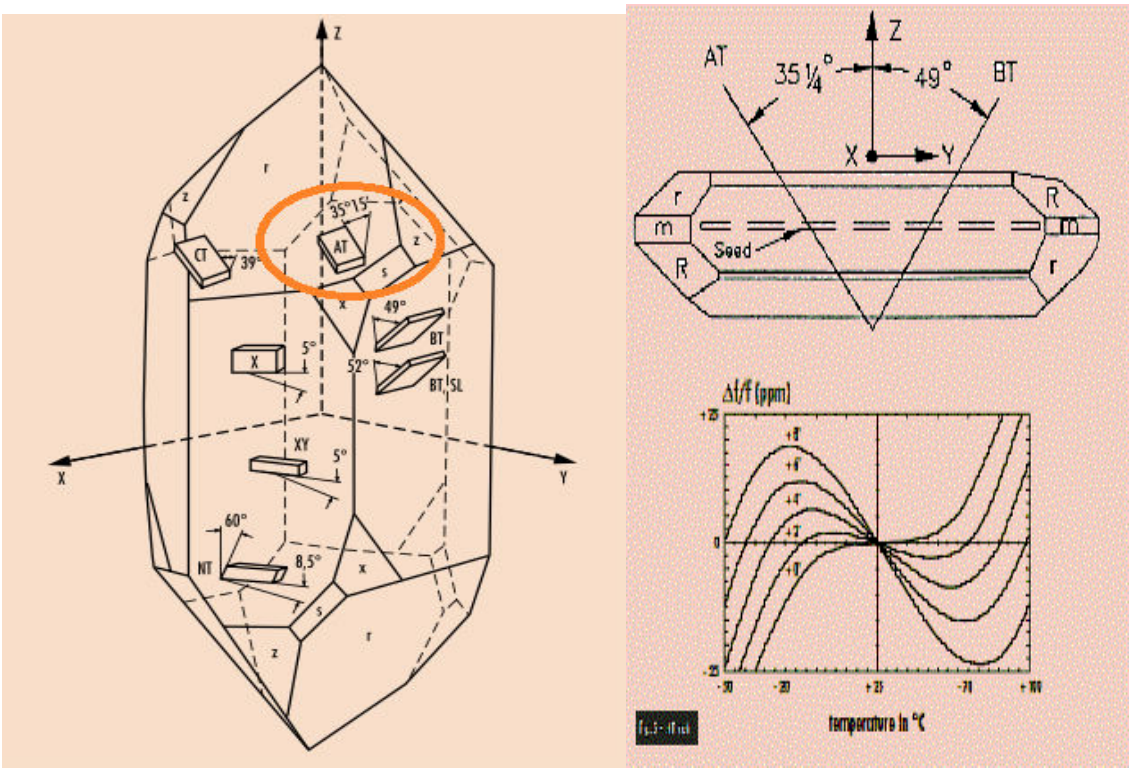

Fig.3.
The quartz crystal and its different cuts (left), AT and BT cuts (top right) and the dependence of the frequency shift in ppms from the resonant frequency due to changes in temperature (bottom right).

In order to relate the change in the resonant frequency of the system due to the addition of some mass at the surface the Sauerbrey equation[6] has been used since 1958. A simplified solution is:

$$\Delta f_s \cong \frac{-2 f_s^2}{\sqrt{\mu_Q \rho_Q}} \frac{\Delta m}{A}$$

Where f_s is the series resonant frequency, μ_Q is the quartz's dynamic viscosity, ρ_Q is the quartz's density and A is the slab's area between the electrodes (piezoelectricaly active). The fundamental frequency, which is be the resonant frequency for the mechanical system formed by the piezoelectric material, can be calculated as:

$$f_0 = \frac{v}{2t_q} = \frac{\sqrt{(\mu_q/\rho_q)}}{2t_q}$$

Where v is the acoustic wave speed in quartz and t_q is the thickness of the crystal.

It is of remarkable importance to indicate that Sauerbrey calculations only apply for solid depositions of layers over the electrode's surface when exposed to air.

The sensor is thought to work surrounded by the analyte (liquid containing the target biomolecules). In order to include the presence of viscous fluids in the system like the analyte, Kanazawa and Gordon equation[7] has been profusely used for large enough liquid layers. It explains the frequency shift of the resonator due to the presence of the liquid.

$$\Delta f = - f_0^{3/2} (\eta_l \rho_l / \pi \rho_q \mu_q)^{1/2}$$

Being f_0 the resonant frequency and η_l the viscosity of the liquid.

When a crystal coated with a thin rigid film operates in a fluid, the interference between mass and viscosity effects is negligible and the problem can be treated in an additive manner. Thus, the shift in frequency appears as the sum of two independent phenomena[8]:

$$\Delta f_r = \Delta f_m + \Delta f_\eta$$

Consequently, shift in frequency measurements are not sufficient to fully characterize the acoustic response of a quartz crystal loaded with a viscoelastic layer due to a mass increment. Another quantity must be considered in order to quantify the energy dissipation. The half-band-half-width named Γ is particularly convenient for this purpose as it enables to generalise the resonance frequency in a complex quantity defined by[9,10]:

$$\tilde{f}_r = f_r + i\Gamma$$

Whose change can be related to the acoustic impedance of the additional layer in the small load approximation by[9,11]:

$$\Delta\tilde{f}_r = \Delta f_r + i\ \Delta\Gamma = \frac{if_0}{\pi Z_{cq}} Z_{layer}$$

Where:

$$Z_{cq} = \sqrt{\rho_q \mu_q}$$

is the characteristic acoustic impedance of the quartz crystal and Z_{layer} is the acoustic impedance of the layer. For a viscoelastic layer of finite thickness, this impedance takes the following form[9,12]:

$$Z_{layer} = i\sqrt{\rho_{layer} G_{layer}} \tan\left(\omega \sqrt{\frac{\rho_{layer}}{G_{layer}}} h_{layer}\right)$$

Where G_{layer} is the complex shear modulus of the viscoelastic material ($G_l = G'_l + iG''_l$)

However, it can be noticed that low viscosity fluids do not disperse the impedance data below 250MHz[13].

Electric analogies can be made for mechanical systems. Electrical conductance measurements against changes in stimulation frequency are key to understand the intrinsic mechanisms of the resonator. Here there are real measurements from another group [14].

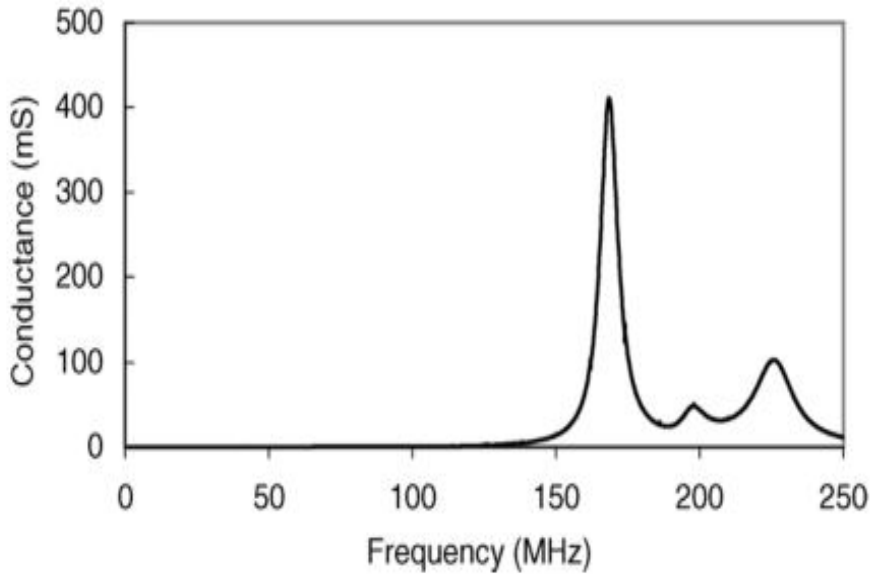

Fig.4. Conductance spectrum of a quartz resonator.

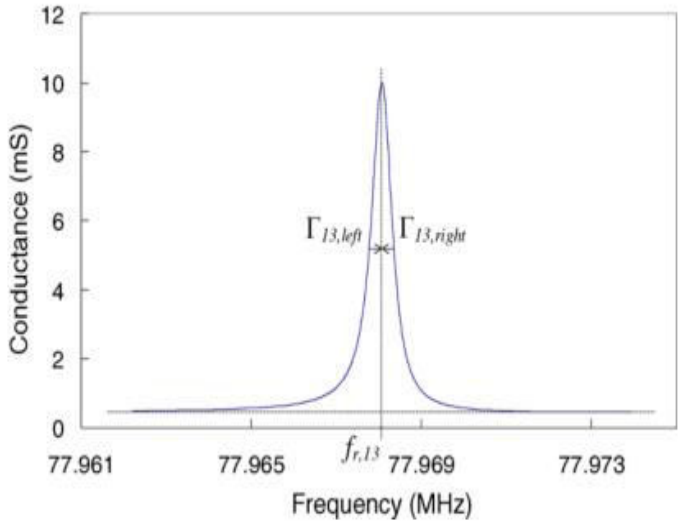

Fig.5.

Viscosity effect illustrated with the conductance spectrum of a 6MHz crystal on its 13th overtone.

Note the dissymmetry in the peak, coming from real scenario conditions later discussed. The dissymmetry of the peaks increases with overtone number[15].

Without measuring the thickness of the adsorbed layer, the mass can not be calculated knowing the other physical parameters. However, it has been proposed a method [15] which implies lowering the temperature until the coupling can be considered rigid to estimate the missing parameter, in this case, the thickness.

Johannssmann[16] proposed another approach to overcome the mathematical complexity arising from the lack of experimental information. It consist in the substitution of the tangent of the impedance by a third order Taylor expansion. This only holds when the layer's thickness is very small, leading to linear functions of the square root of the overtone number "n":

$$\frac{\Delta f_r}{f_r} = -\frac{8\pi^2 f_0^3}{3Z_{cq}} \frac{m_f^3 J'_f}{\rho_f} n^2 - \frac{2f_0}{Z_{cq}} m_f = a_f n^2 + b_f$$

$$\frac{\Delta \Gamma}{f_r} = \frac{8\pi^2 f_0^3}{3Z_{cq}} \frac{m_f^3 J''_f}{\rho_f} n^2 = a_\Gamma n^2$$

Where m_f is the mass per unit area of the film and J_f is the shear viscoelastic compliance ($1/G_f$). $J_f = J'_f - iJ''_f$

Unfortunately, the real behaviour of crystal resonators is subjected to several effects disregarded by this model such as quartz anisotropy, finite crystal boundary conditions, piezoelectric stiffening, energy trapping and anharmonic resonances.

SHEAR WAVE IN A SEMI-INFINITE FLUID

The simplest model to address the behaviour of viscous fluids in contact with the shear resonator includes the use of the conductance vector G. Its real component, G', represents the elastic constant of the material, while its imaginary part, G'', represents the viscous energy losses. When a material is perturbed with an angular frequency ω, the tangent of losses α=G''/G' represents the amount of energy lost as heat in each cycle of the material perturbation.

In the case of rigid materials, G''->0 and α–>0, so all the energy is stored in the material, behaving like a "spring" as hard as high is G'. On the other hand, in perfect newtonian liquids, G'->0 and α–>∞, so no energy is stored at all and is rather spent in the viscous agitation of the fluid having a viscosity η=G''/ω. It is important to note that G' and G'' are dependent on ω, in the sense that a fluid showing newtonian characteristics at some frequency can behave a a rigid solid at other frequency. This happens because of the dependence of some molecular properties of the material, expressed as macroscopic parameters, on the time scale in which the perturbation produced.

For viscous fluids, we can find Sauerbrey like behaviours when the thickness of the fluid is very small. On the other hand, when the layers are thick enough, we enter the Kanazawa zone, behaving like a semi-infinite liquid. For intermediate thicknesses the behaviour is more complex as it neither follows Sauerbrey nor Kanazawa approximations.

Here is a figure showing the evolution of a newtonian fluid expressed through the equivalent electric impedance of the liquid film Z_f as the thickness is increased, considering its real and imaginary components, namely the real part R_f (resistance) and the imaginary part X_{Lf} (inductance)[17]

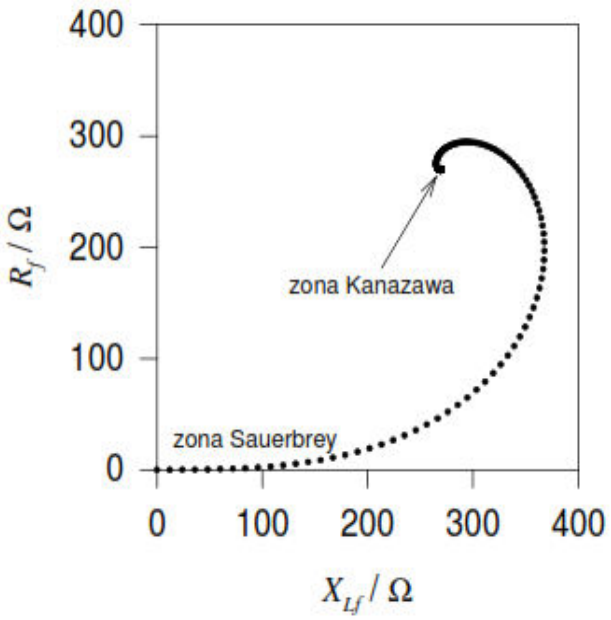

Fig.6.
Impedance parametric evolution with increases in liquid layer thickness.

Note the evolution of the electric impedance against thickness "d", going from the linear Sauerbrey behaviour to the independence from d in the Kanazawa zone.

Bearing in mind the medium properties, it is possible to model the behaviour of the shear waves induced by the resonator inside the fluid. To simplify the model an incompressible fluid is are considered.

Here there is a scheme of the oscillatory flow and the deviatoric stress state on a infinitesimal fluid element:

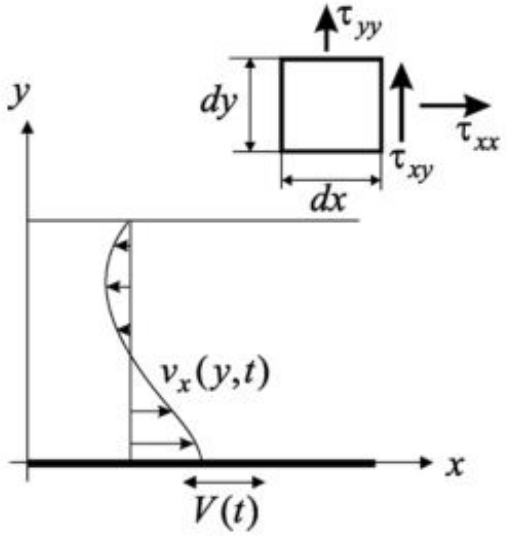

Fig.7.
Oscillatory flow due to the movement of a plane and deviatoric state of a differential element.

The modelling of a shear wave inside sputum is extremely complicated. However, a sample preconditioning step before the measurement is expected. This means the sensor will not face sputum directly, instead, it will face diluted sputum in some organic solvent (similar to the model proposed). The mathematic appearance of the shear waves in a semi-infinite linear viscoelastic fluid is as follows [18].

Taking into account the no-slip condition and the far-field boundary condition ($v_x(y=0,t)=V(t)$ and $Lim_{y->\infty}(v_x(y, t))=0$, respectively), the velocity field within the liquid is:

$$v_x(y,t) = \mathrm{Im}\{e^{it}\, e^{-\delta y}\} = e^{-\alpha y}\sin(t-\beta y)$$

Where $\delta=\alpha+i\beta$, $1/\alpha$ is the penetration length scale (until extinction of the perturbation) and $2\pi/\beta$ is the oscillation length scale. Note that v_x is a non-dimensional variable (time is expressed as $\tilde{\omega}^{-1}$). The Reynolds number determines both variables through $\alpha=\beta=\sqrt{Re/2}$ with $Re=\tilde{\rho}\tilde{\omega}\tilde{A}^2/\tilde{\eta}_0$.

As discussed before, for the device to work properly, it is needed to obtain the vector G experimentally for the analyte using the expressions:

$$G' = \frac{\left(\beta^2-\alpha^2\right)Re}{\left(\alpha^2+\beta^2\right)^2}, \qquad G'' = \frac{2\alpha\beta Re}{\left(\alpha^2+\beta^2\right)^2}$$

By rewriting the expression in physical terms, the formulas of Ferry et al. appear [19]:

$$\tilde{G}' = \tilde{\rho}\tilde{\omega}^2\frac{\left(\tilde{\beta}^2-\tilde{\alpha}^2\right)}{\left(\tilde{\alpha}^2+\tilde{\beta}^2\right)^2}, \qquad \tilde{G}'' = \tilde{\rho}\tilde{\omega}^2\frac{2\tilde{\alpha}\tilde{\beta}}{\left(\tilde{\alpha}^2+\tilde{\beta}^2\right)^2}$$

In this equation the dependency of the G vector on the angular frequency is revealed. Its relationship with the actual viscosity $\eta=\eta'-j\eta''$ (being η' the dynamic shear viscosity and η'' the out-of-phase viscosity, also named elasticity) follows this expression [13]:

$$\eta = -j\frac{G}{\omega} = \frac{1}{\omega}\left(G'' + jG'\right)$$

ELECTRIC MODEL

The elaboration of the electrical model begins with the theorization of the circuit diagram. Butterworth-van-Dyke (BVD) equivalent circuit is widely used in the literature [20] and its graphical representation is:

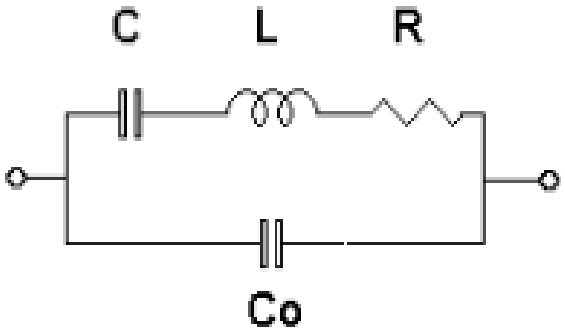

Fig.8. Representation of the equivalent electric circuit.

There exists a principal branch called "mobile" or "series" (RLC), which represents the acoustics of the quartz crystal and its electrodes. In parallel to this branch there is a parasitic capacitance C_0 representing the actual electric capacitance in the electrodes-quartz system, and thus does not stand for any mechanical compliance. Each component in the series branch addresses different phenomena within quartz resonance. C is the mechanical compliance of the quartz, L is the inertial component of the electrodes-quartz system and R stands for the energy losses during resonance.

Based on the impedance spectrum analysis of the COMSOL model (by Luis Armando Carvajal at CTB-UPM) calculations were made in monophasic circuitry modelling programs to design the circuit. The values for the different elements were estimated to maintain the same impedance behaviour in frequency as the *in silico* experiments.

The resonant frequency f_r and the half-width-half-maximum can be calculated as:

$$f_r = \frac{1}{2\pi\sqrt{L\ C}}$$

$$\Gamma_n = \frac{R}{4\pi L}$$

However there is also a way to graphic the data using the admittance Y(Y=1/Z) in order to obtain the values of R, C, L and illustrate at the same time the effect of the real electric capacitance C_0 [17]. Y can be expressed as the sum of its components, "G" conductance and "B" susceptance.

$$G = R / (R^2 + X^2)$$

$$B = X / (R^2 + X^2) + \omega C_o$$

$$X = \omega L - 1/\omega C$$

$$\omega_s = 2\pi f_s = (LC)^{-1/2}$$

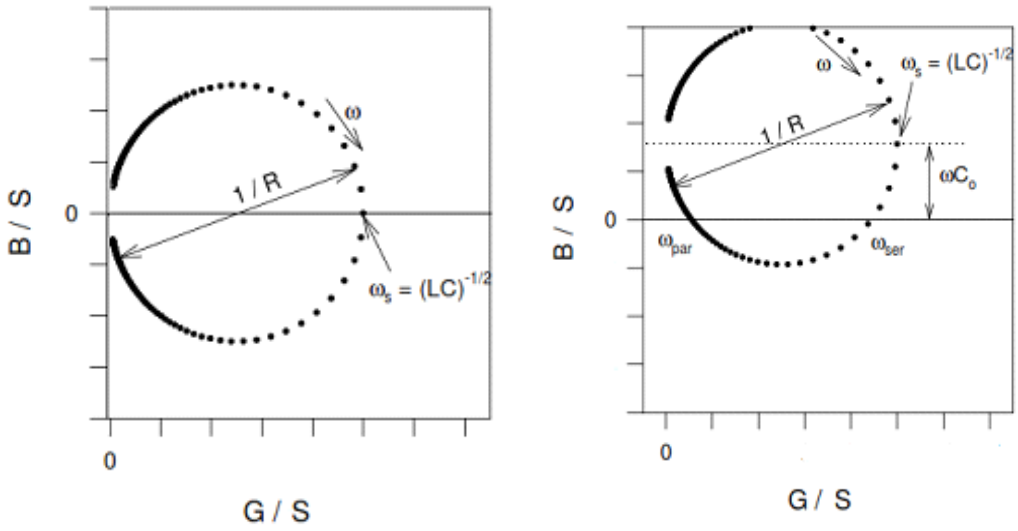

Fig. 9.
Evolution of admittance in frequency with and without considering the electric capacitance of the system electrodes-quartz.

These are the cases for C_0=0 and C_0 different from zero. In the second case, the value for ω with phase=0º (B=0) is displaced, both the series and the parallel angular frequencies. It is important to comment the effect of C_0 regarding the total behaviour of the system. As C_0 is increased both frequencies tend to collapse in the same value. When ωC_0>1/2R the system does not resonate any longer.

The quality factor Q is of paramount importance regarding frequency resolution of the acquired signal. In an ideal RLC circuit the quality factor can be calculated as:

$$Q = \frac{1}{R}\sqrt{\frac{L}{C}}$$

It can also be approximated by the expression [13]:

$$Q \approx \frac{1}{\left(R_Q + R_L\right)}\sqrt{\frac{L_Q + L_L}{C_Q}}$$

Where: R_Q is the resistance of the quartz, R_L is the resistance of the layer in terms of energy dissipation, $L_Q + L_L$ represent the inertial mass of the system quartz-layer.

This information is enough to build the model provided an estimation of one parameter. The most restrictive element in terms of dimensions and prices was, in this case, the 250μF inductor. Also, it is a critical factor in the establishment of a proper resonant frequency in the circuit. Bearing this in mind the following circuitry was built using a welder, Sn, and a Cu connection board.

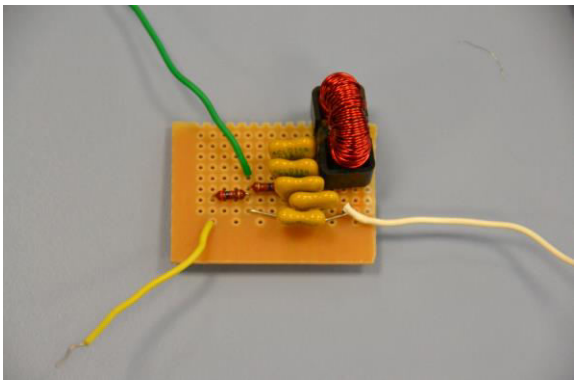

Fig.10. Equivalent electric resonator.

In this image the final circuit is shown. All the components at the right from the first resistor represent the quartz resonator. White is ground, yellow the excitation signal and green the probe for assessing the behaviour of the resonator. The lower capacitor stands for the electrical capacity of the resonator while the rest of the resonator equivalent represents the mechanical behaviour.

This is the scheme of the electric model together with the excitation signal. Here the series branch is found on the far right and the electrical capacitance is represented by C0. The resonator probe is positioned as shown below in order to observe in the oscilloscope the state of the resonator.

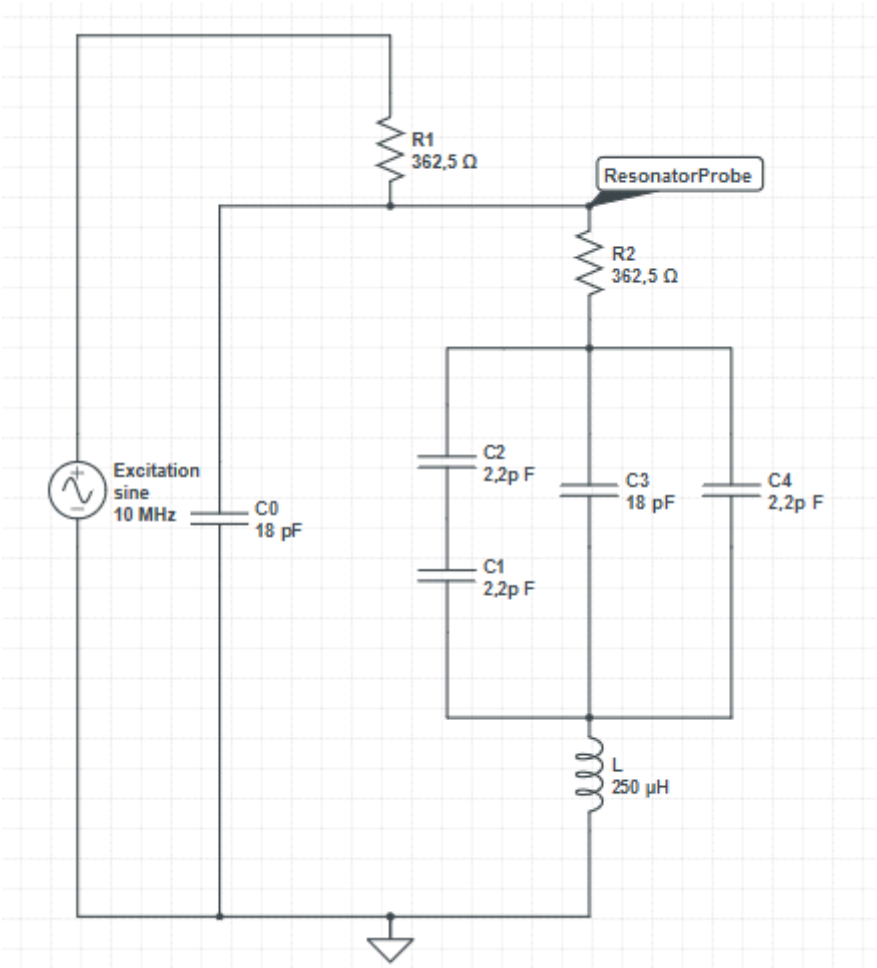

Fig.11.
Schematic representation of the electric circuit.

Here is a list of the components used in the circuit:
-Two 362,5 Ohm resistors.

-Two 18pF capacitors

-Three 2.2pF capacitors

-One 250µH inductor

The circuit was probed with an analog oscilloscope and then fed with a frequency tuneable $10V_{pp}$ sinusoidal signal in order to check the resonant frequency of the circuit.

DISCRETE MODULATION (NARROWBAND SIGNALS)

In the next lines a system for discrete amplitude modulation is explained[21], in which the signals are considered periodic, namely, the modulating signal x[n] and the carrier signal c[n]. The bases of this method are the Fourier transform and its properties:

$$\mathcal{F}\{f\} \quad : \xi \mapsto \hat{f}(\xi) := \int_{-\infty}^{\infty} f(x)\ e^{-2\pi i \xi x}\,dx,$$

The properties arising from the study of continuous time signals are also valid for discrete time signals (specifically the property which indicates that the multiplication in the time domain is the convolution in the frequency domain). Here, the function named with a capital letter as function of a complex exponential is the Fourier transform of the small case function.

$$y[n] = x[n]c[n]$$

$$Y(e^{j\omega}) = \frac{1}{2\pi}\int_{2\pi} X(e^{j\theta})C(e^{j(\omega-\theta)})d\theta$$

The carrier has an special shape in the Fourier domain. In the time domain it exists as a complex exponential while in the frequency domain it turns out to be a train of deltas.

$$c[n] = e^{j\omega_c n}$$

$$C(e^{j\omega}) = \sum_{k=-\infty}^{+\infty} 2\pi\delta(\omega - \omega_c + k2\pi)$$

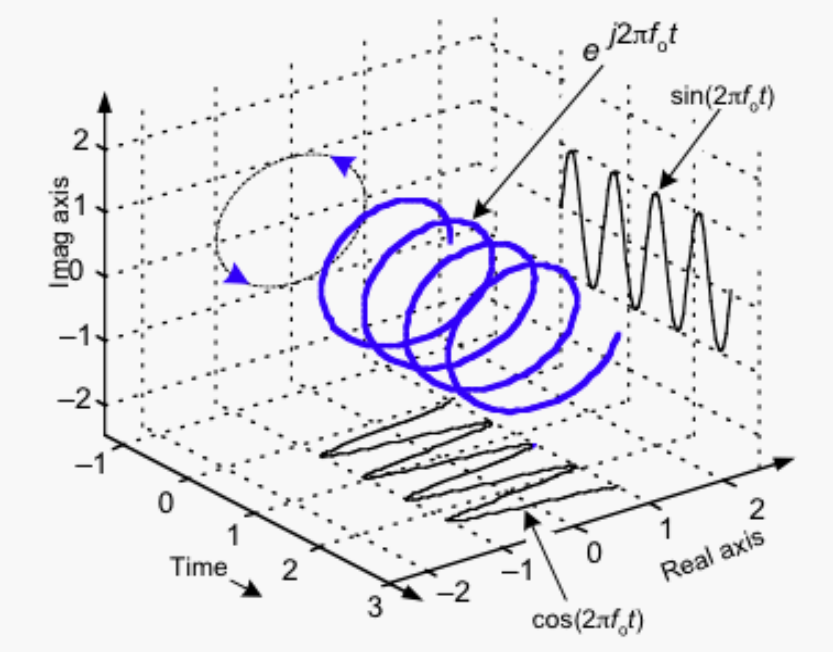

Fig.12. Continuous time complex exponential function.

This is an illustration of a continuous time complex exponential, whose discrete form is used in this case as the carrier.

This relationship between the complex exponential and its real and imaginary parts is well is well understood through the trigonometric circle. This is the origin of the so called Euler's Formula.

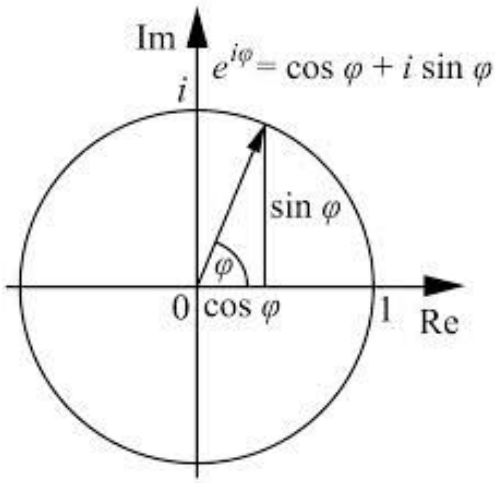

Fig.13. Trigonometric circle.

The delta-train shape of the Fourier transform of a signal like this added the properties of the Fourier transform are ideal for sampling purposes. The convolution of this train of deltas with other periodic function will displace ω_c in frequency the original spectrum. In this way the system would work as follows:

Considering the form of x[n] and c[n] in frequency domain:

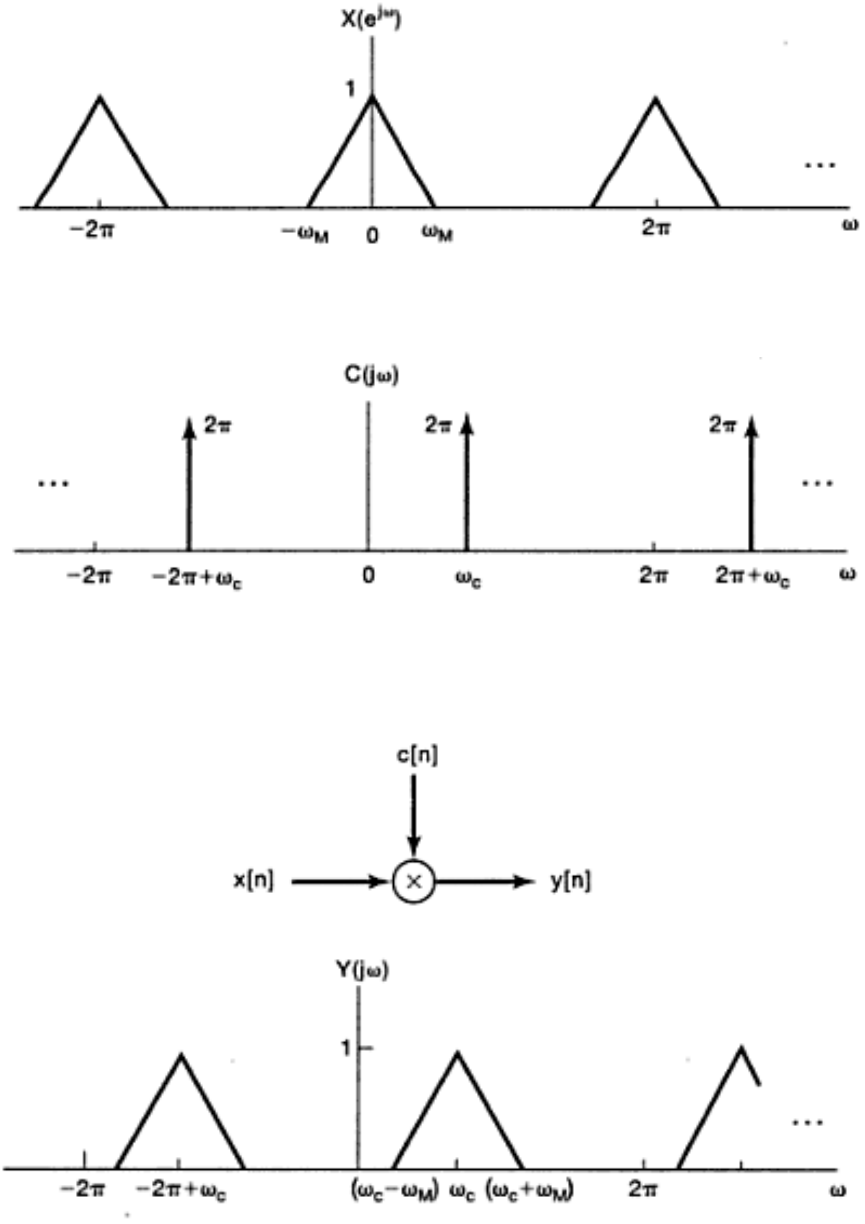

Fig.14. Sampling with Fourier tranform.

Note that in order to recover the signal, it must be fulfilled that:

$$\omega_M < \omega_c < \pi - \omega_M.$$

Remember that Y(jω) is the convolution of X(jω) with C(jω). The resulting function is just a displaced version of the original spectrum of the modulating signal.

In the case of this sensor, the signal generated is a sine with some of its harmonics its harmonics and noise. The signal spectrum is a series of peaks which decay exponentially in magnitude with the distance to the central one, situated at the signals frequency. In a simplified version of the signal we can consider it as a pure sine, which Fourier transform will be just an anti-symmetric pair of deltas.

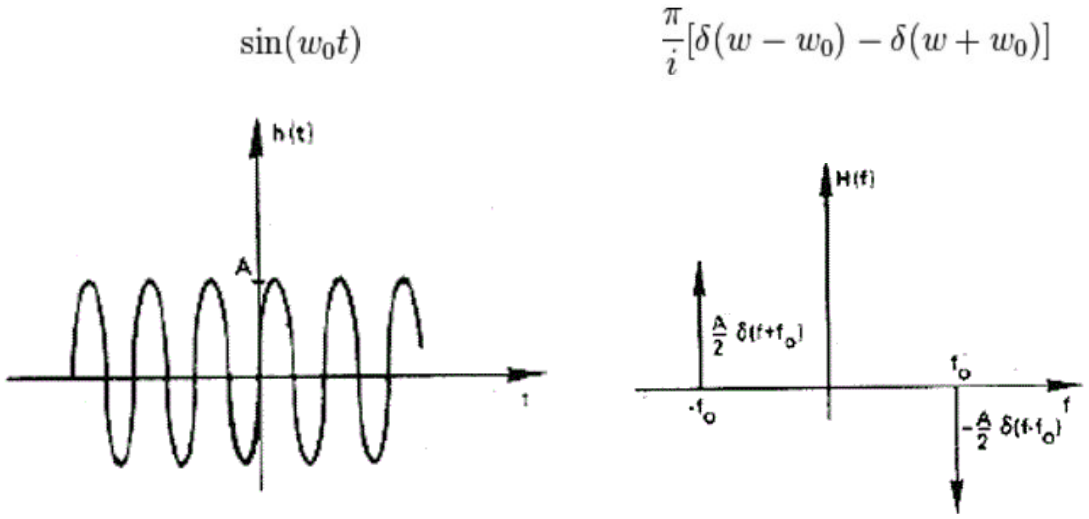

Fig.15.
Sine function and its Fourier tranform.

This would mean an ideal narrowband signal. In the real case this peaks will have a defined bandwidth, although small enough for modulation purposes taking into account the Nyquist theorem (f_s>=2*bandwidth).

CHAPTER 3. RESULTS

THE CASE

Here are some images of the case made with SketchUp (note that in order to get some resolution within the programme, ten millimetres of the SketchUp design are one of the real model)

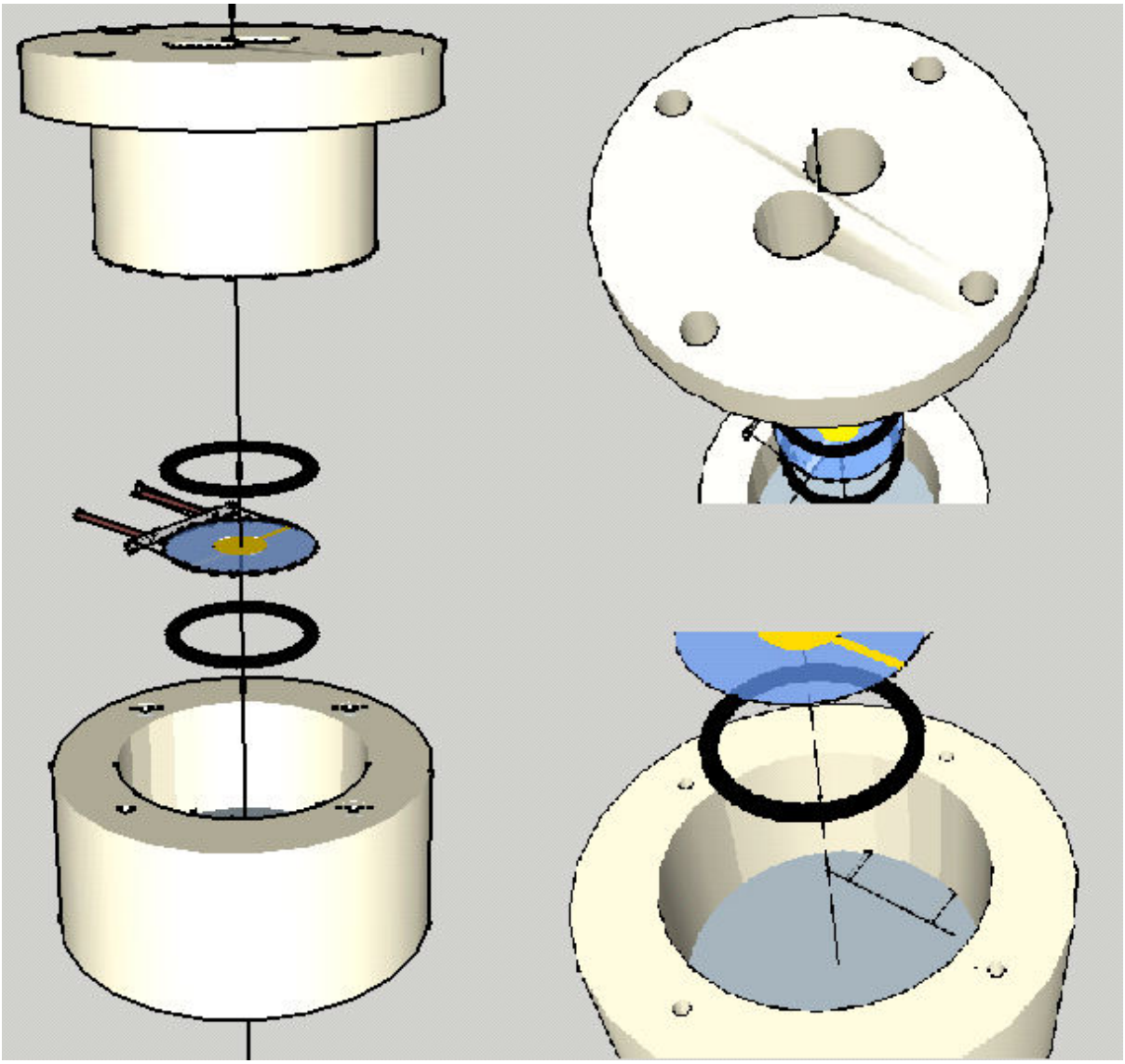

Fig.16.
Images of the whole case (left), the cap (top right) and the support (bottom right).

In the left view we can see the general arrangement of the QCM and the case. Following what appears in the literature, O-rings were thought as suitable mechanical support. The top right image shows the capping of the system. Two big cylindrical holes were drawn for the inlet and outlet connections. Typical size screws were considered to be used and the pertinent orifices were created.

In the bottom right image it is shown the supporting system. It has cavities for the screws and prismatic holes for the electrode connections with the piezoelectric. It also includes (as does the cap) small features for the isolation of the piezoelectric to steadily fit inside the case.

NATIONAL INSTRUMENTS DATA ACQUISITION CARD (USB-6351)

Thanks to the simple user interface and its ease of setup, the card was quickly installed in the PC. This card had several channels for analog and digital signals. The drivers were so that no further modification was needed to use it within LabView as both products are from the same company. Anyhow, the maximum sampling frequency supported by the DAC was 1,25 MS/s (1,25 million samples per second). This was a great disadvantage as this digitalization setup seriously restricted the acquisition of the interesting signals (~10MHz). Furthermore, all efforts were made in order to accomplish reliable data acquisition for one channel, which would be tremendously difficult for two channels as it would be necessary to access the internal clock of the central processing unit and couple it to the DAC (the final system may work in parallel with another reference sensor).

VIRTUAL INSTRUMENTS IN LABVIEW

The first experience with LabView after its installation was getting familiar with the programmes functions. After being able to generate a virtual band-pass 2nd order Butterworth filter (99900-100100 Hz) and test it against different digital signals generated *in silico*, the filter was connected to a function generator. After feeding white noise to the digital filter, it was observed the well functioning of the filter.

Then the next step would be to acquire a pure sinusoid signal in the range of the 10MHz coming from the function generator. This was challenging due to the fact that this frequency was approximately ten fold that of the sampling frequency in the DAC. This is when narrowband width signal demodulation comes into play. Being the minimum period measured by the DAC 0,8 microseconds, it was then needed to develop a sampling criteria which would not exceed this limit. Then a carrier signal was used to be modulated by the one coming from the generator.

The carrier, after some conservative calculations, was set to have an angular frequency of 24960Hz (around the fifth part of the maximum sampling frequency in the DAC) which was approximated to 25kHz. The results were

good, with high temporal resolution, but the acquisition time was not optimized. After using 990,099kHz as the sampling frequency (less than the max sampling frequency) and adjusting the band-pass filter, the results were optimized for one channel. More than one analysis of the input signal frequency were carried out each second.

Here are both, an image of the virtual instrument on LabView and an image of the users display:

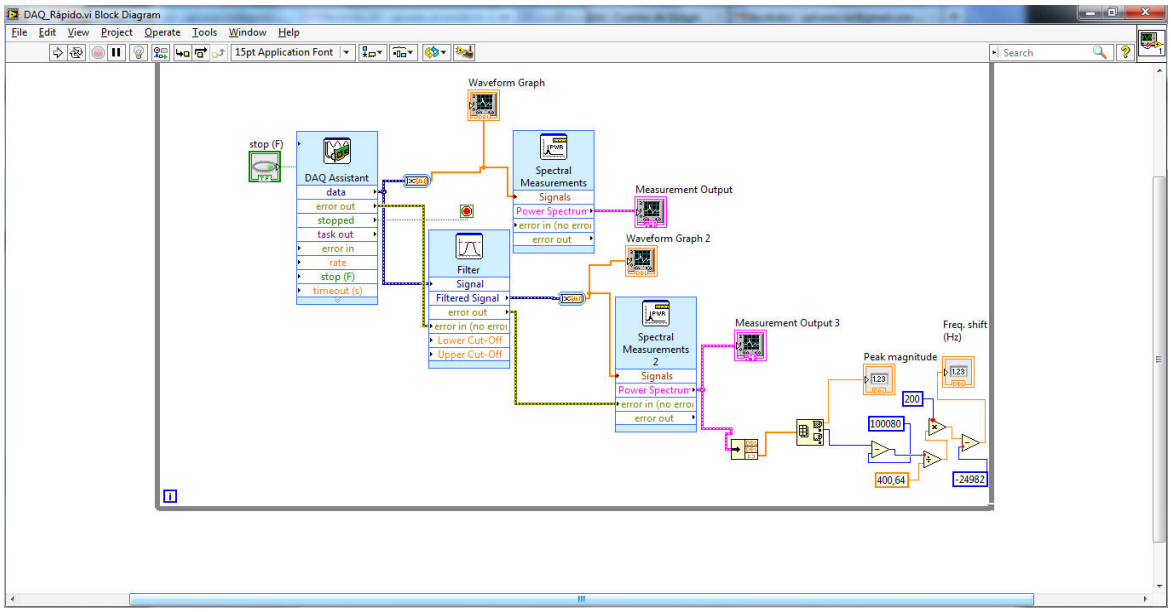

Fig.17.
Image of the virtual instrument created for data analysis.

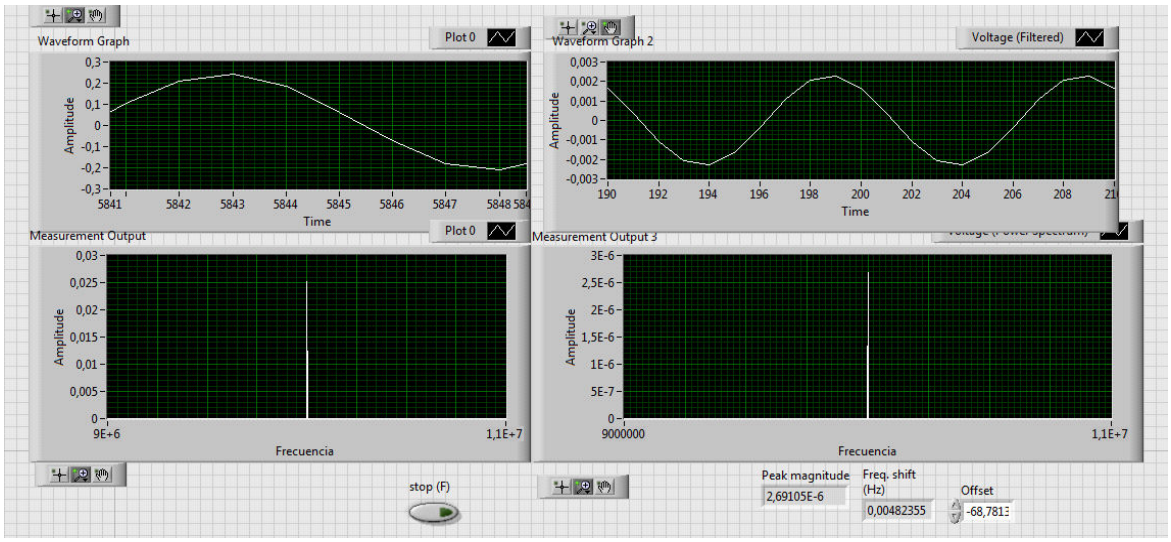

Fig.18.
Image of the data display.

Other approaches were studied and implemented. In order to lower the noise in the signal coming from pseudo periodic events in the real scenario, it

was intended to randomize the carrier signal; this is sampling at random increments of time within some working limits to discard events occurring at the sampling frequency.

Also it was tested the possibility to excite a real sensor with the PC. Making use of the DAC, whose maximum sampling frequency was 1,25MS/s, it was impossible to continuously recreate a 10MHz sinusoid for excitation of the analog circuit.

ELECTRIC MODEL TEST

After the tests carried out only using the function generator, the electric circuit equivalent to the piezoelectric system was built. Luis Carvajal supervised the whole building procedure. Based on the theoretical calculations using monophasic circuitry modelling programmes, the components were bought from RS Components International, being the inductor the most expensive and restrictive (250μH).

The circuit described above, was fed with a $10V_{pp}$ and 10MHz sinusoidal signal. The system was probed by potential difference at the ends of the pseudo-piezo component (ResonatorProbe illustrated in the schematic of the circuit) with the analog oscilloscope, including the capacitance components coming from the theoretical intrinsic capacitance to the dielectric layer of the capacitor. The digital oscilloscope was useless here as it had not enough time resolution to make the calculations needed in real time. Problems were observed without capping the power supply to 20MHz, probably due to over excitation of overtones inside the crystal and spurious modes close to the resonant frequency. The observations were clear that the resonant frequency of the model was 10MHz as expected, measuring when the phase between the excitation and the resonance was 0º.

Here is an image of the analog oscilloscope screen:

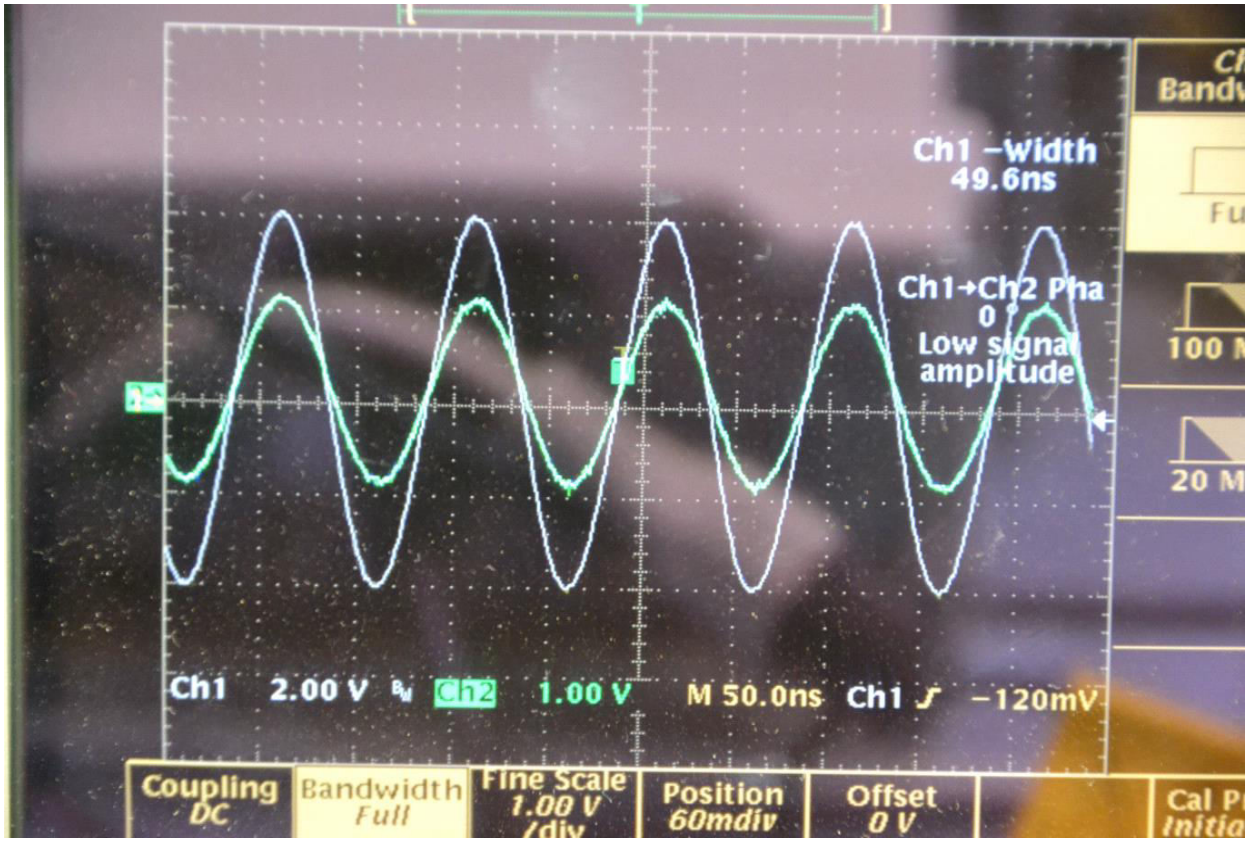

Fig.19.
Picture of the analog oscilloscope screen at resonance of the electric equivalent.

Note that: Ch1 is the power supply, Ch2 is the signal coming from the pseudo-quartz and the frequency in the image is 10MHz (T=99,2ns).

It was pleasant to observe in real time the behaviour of the model at difference frequencies. At really low frequency the system behaves like a pure resistor. Then, with increasing frequency, capacitive behaviour takes the lead while inductive reactions begin to appear. After crossing the 0º phase point, at which resonance occurs, if frequency was increased further more the induction takes it all, producing a 180º phase signal of low voltage.

CHAPTER 4. DISCUSSION

THE CASE. FABRICATION AND MATERIALS

While all the programmes involved were being installed in the PCs available in the laboratory, the design of the external case was theorized. The material to be used was theorized taking into account requisites such as size, smallest feature resolution, and anti-fouling properties of its surface. In this manner, PMMA ((Poly(methyl methacrilate)) was found to be suitable for this case. Its intrinsic inexpensiveness and its cheap sculpting with enough resolution (by CO2 laser) make it a clear candidate for low-cost batch fabrication. Also it shows little adsorption of DNA and proteins (which could be deleterious for the acquired signal). However, regarding other further functionalities of the biosensor to be added, it is to be known that PMMA show some auto-fluorescence (which could disenable different kinds of *in situ* optical measurements). Furthermore, its glass transition temperature (105 ºC) and its high thermal expansion coefficient, interdict any high temperature operation regime. Although raster scanning is a time consuming technique, the use of advanced digital mirror devices could help keeping the fabrication time per unit extremely low.

Several designs in literature were studied and compared in order to create a simple model for further experiments. Although the free ScketchUp version was used, the file can be opened in the pro version. This would allow to create objects called "solids" so their internal volume would be also considered by the programme. With this new file, Slic3r can be used to create arbitrary binary tomographies, which can later be fed to a 3D printer to create a prototypical case for experiments at the laboratory. As the smallest feature is around one millimetre, this can be challenging for many DIY deposition 3D printers available. The model is still to be tested in a real scenario.

VIRTUAL INSTRUMENTS IN LABVIEW. OPTIMIZATION

The method developed has theoretically enough time resolution regarding the nature of the biomolecular complex formation and detection. All the measurements obtained have an error below 1% of the theoretical value. It is remarkable here that the aim by this time of the work was to have enough frequency resolution of the signal. With this method, differences of 1Hz were successfully measured in the PC as the signal from the function generator was

varied. In theory, the differences created by the addition of biomolecules on a viscous film of a few tens of nm, is in the order of the kHz.

In order to get rid of noise in the real scenario, the other modes of the piezoelectric should be considered to suppress the harmonics in the signal. Although this crystals show a great behaviour in air, they see reduced their quality factor due to the viscosity of the medium. In frequency this will be a broadening in frequency of the peak detected. Its is also important to remark that shear waves inside the analyte are only able to travel a few hundreds of nm. This will prevent them from coming back to the piezoelectric surface and complicating the signal. In any case, if the aim of the final device is to give a qualitative measurement regarding only one bacterial family, the signal to be measured would have a much larger magnitude than the noise considered.

The use of hopping-frequency sampling was promising but required four times more waiting between measurements. However, this possibility should be considered regarding the real scenario noise sources.

Experiences with signal generation from the DAC aiming a real quartz sensor indicate us the incompatibility of continuous mode excitation methods with our digitalization set up. However, the spacing between excitation sequences can be affordable measuring the decay constant for viscosity estimations. This is due to the fact that excitation and measurement need to be synchronized, allowing the system to prepare the signals in the meantime.

ELECTRIC MODEL. NEXT STEPS

Although results were surprisingly similar to those expected theoretically, it must be considered for the real case scenario that the medium itself would represent an increase of this capacitive component, represented in the model as a parallel capacitor.

The theory involved indicates that the viscosity of the medium can be modelled changing the resistance in the circuit. This can be achieved with an increase in resistance proportional to the increase in viscosity, calculated in terms of energy dissipation.

The previous experiences with the digital oscilloscope indicate that a digitalization phase regarding measurement, filtering and calculation may increase the acquisition time and price of the final device.

Further work could be focused on the emulation of different physical media and conditions within the electrical model. In order to do so, a tuneable

inductor and a simple potentiometer could be used to emulate different media. This data could be also compared to existing experimental data, providing potential useful analogies with the real scenario for system calibration.

ELECTRODE BIOFUNCTIONALIZATION

Here it will be discussed the use of Self Assembling Monolayers together with the QCM technology as a new approach for electrode biofunctionalization. The information below was studied in class during the BioMEMS course in the UC3M, addressing the lecture about micropatterns of SAMs, given by Cristina Sánchez López de Pablo. Notions from the course about Nanotechnology in Biomedicine were also applied.

These layers are formed by ethileneglycol polymers with reactive groups at its ends, being able to form a nanosized layer of material over a substrate. The resulting interface can be impermeable to proteins and water by adding Acrylamide chains on the substrate before adding the PEG chains. This is due to the formation of the so called interpenetrating networks within the layer.

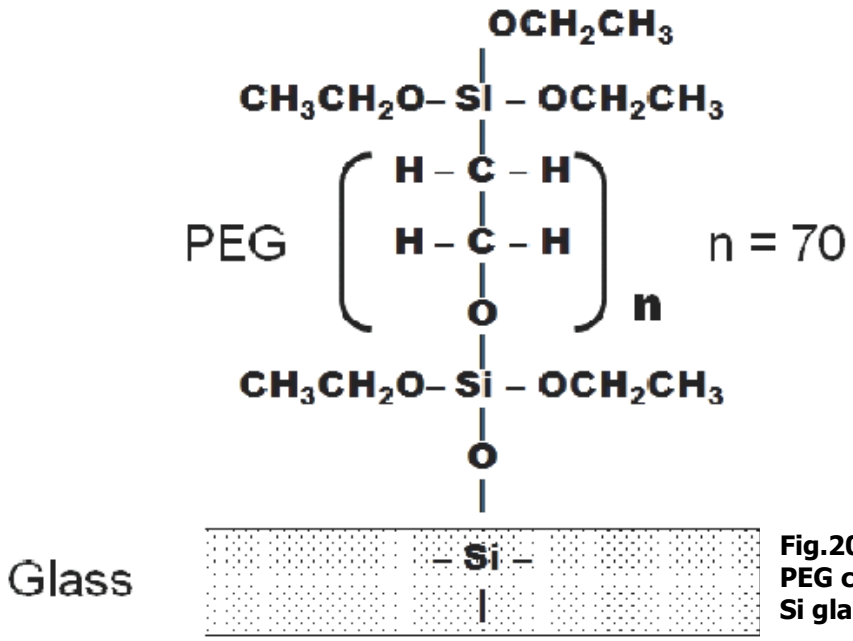

Fig.20. PEG chain over Si glass.

The viscosity of this layers depends on their thickness, which is determined by the number of monomers in each chain. This number can be varied during the synthesis of the PEG chains. If the length is too large, the molecules surrender to thermal noise, collapsing the brush conformation. On the other hand, if these chains are too short, the interaction with the substrate would be higher than between chains, resulting in the adsorption of the chains and consequently hindering the brush conformation. The vertical disposition of

the chains is critical regarding the complete exposition of the active recognition site of the receptor biomolecule. This disposition could be achieved designing a reaction targeting the N-terminus of the peptides involved. In the case of DNA, phosphodiester bond would be a good strategy to confine the bioreceptor on the exposed surface .

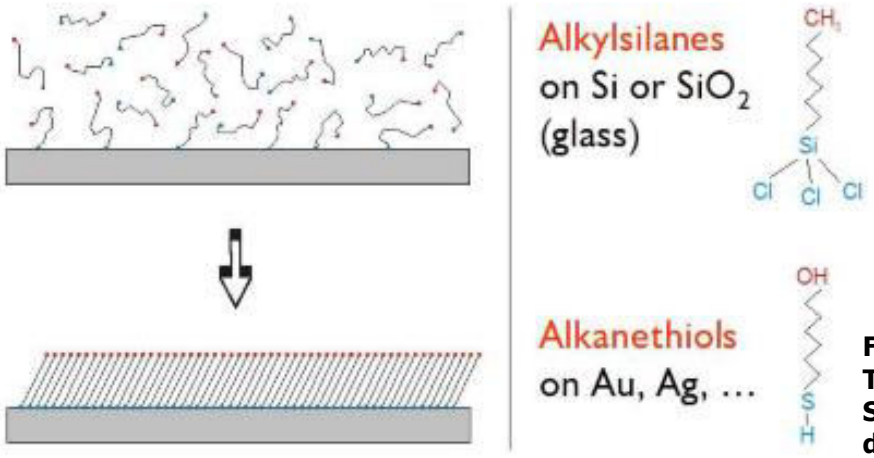

Fig.21. Types of SAMs for different substrates.

In terms of the physics behind, the addition of this layer would mean a third phase through which the acoustic waves are propagating. In the electrical model, this could be calibrated with the addition of a resistor in series with the resonator, mimicking the effect of the viscosity in terms of energy dissipation. However, the resonant frequency depends mostly on the inertial and capacitive components, being Q, the quality factor, the only one affected (reduced in this case). The calculation of the total mass and compliance of the SAM can be estimated depending on the length of the individual chains, calculations required for the optimization of the device.

The synthesis of SAMs has been profusely investigated. It basically involves some basic organic chemistry. In this case, the addition of the bioreceptor molecule should be kept in mind for the design of the synthetic procedure. Also, the phisio-chemical reactivity of the SAM against the analyte solution should be taken into account. Alkenethiols seem to be a good approach for gold electrode biofuntionalization. The thiol groups at the end form a dative bond with the metallic surface, acting as an anchor.

In any case, there is the need for a medium length crosslinker between the bioreceptor molecules (disposed outwards from the electrodes surface) and the electrodes surface.

The combination of well known gold-micropatterning techniques with microfluidics systems could allow the multiplication of the channels on the quartz surface. This means the assembly of several SAMs forming a biosensors array, presenting different bioreceptors for different measurements. From the literature it is known the promising results of Multichannel-QCM[5].

Here are some illustrations of the device and a real picture of a gold micropattern:

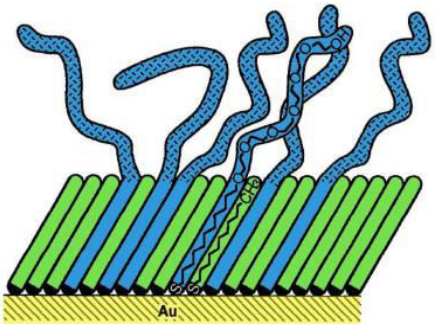

Fig.22.
Schematic of the SAMs.

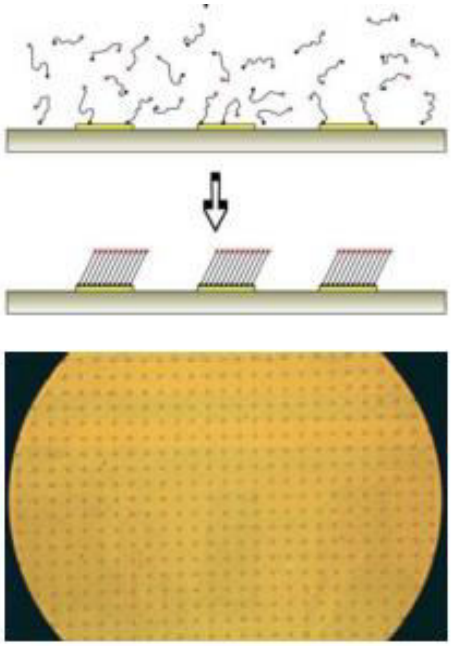

Fig.23.
Schematic micropatterned SAM and real gold micropaterning picture.

Regarding the use of SAMs as a biofuntinalizing agent, several tests can be performed to asses the homogeneity and functionality of the biofilm. At some point, Atomic Force Microscopy (AFM) appears as a required technique for this purpose. However, using Green Fluorescent Protein (GFP) reporter systems can be an inexpensive alternative provided the availability of a fluorescence microscope (household equipment in a cell biology laboratory). The test in this case would consist in checking the homogeneous distribution of a fluorescent reporter over the film provided the attachment to the target molecule.

CHAPTER 5. CONCLUSIONS

DATA ACQUISITION

This method is compatible with the observation of small mass increments during the adhesion of molecules, which only represent a change in the position of the peak, leaving its bandwidth almost intact. Furthermore, if the biological detection is performed using a functionalized self-assembling monolayer, we can make use of a Sauerbrey like approximation, considering the film as almost rigidly coupled to the electrode due to the small thickness of the chains (~24nm for a PEG n=70) and thus simplifying the calculations down to the viscoelastic effects of the liquid around the sensor. However, the solvent used to form the analyte solution should be characterized beforehand to recalibrate the system. Other interesting approach to bypass this lack of experimental data would be to place a bioinactive second sensor inside the medium so it would provide a reference of the viscous effects of the analyte. This effect can be estimated effectively with the Kanazawa approach.

It must not be forgotten the fact that low-cost systems for qualitative diagnosis should be as simple as possible. Regarding data acquisition, outstanding high mass sensitivity and temporal resolution can be sacrificed, reducing the electronics and costs involved.

EXCITATION METHODS

Other excitation methods are used within the field of QCM such as the pulse excitation and the decay measurement. The first approach shows promising results[5] regarding quality factor and the associated signal to noise ratio of the measurement. The later involve the estimation of the decay constant of the signal modelled as $Ae^{-Dt}\sin(wt)$. This D is related to the viscosity of the medium (in this case the biofilm plus the medium). In order to do so, a better coordination between the power signal and the digitalization card is needed to precisely probe the viscous phenomena in between. However, the intrinsic sequentiality of this measurement allows the proposed digital set up to prepare the signals for excitation, being also suitable for this technique.

Despite the benefits in signal acquisition and sensitivity of these alternative methods, the excitation pulses shape is difficult to acquire, involving more and more sophisticated circuitry in the device. Clinging to a simple analog

set up inspired in the optimized digital version would reduce the costs in terms of number of components and ease of fabrication.

It is of remarkable importance the availability of the data required beforehand in the design of the device. Parameters like thickness of the biofilm, its complex shear modulus and physical properties of the analyte should be established to reduce the amount of feedback, electronics and circuitry within the device.

It is left to say that the proposed system could also be used to asses the properties of different media. Regarding its frequency sensitivity, small changes in the resonant frequency coming from the medium alone can be measured. Many efforts are made today looking for reliable measurement of the physical properties of human fluids such as viscosity or density. For example, there is a growing tendency to measure glucose indirectly by how it affects the viscosity of its environment (sweat, interstitial fluid, tears), looking for a non-invasive constant monitoring of the glucose levels in blood.

References:

1. [1] Vademecum.es
2. [2] W.P.Mason, W.Baker, H.J.McSkimin and J.H.Heiss, Physical Review, 75, 6, (1949), 936-946
3. [3] Multichannel monolithic quartz crystal microbalance gas sensor array. Jin X1, Huang Y, Mason A, Zeng X. Anal Chem. 2009 Jan 15;81(2):595-603. doi: 10.1021/ac8018697
4. [4] Quartz crystal microbalance with dissipation coupled to on-chip MALDI-ToF mass spectrometry as a tool for characterising proteinaceous conditioning films on functionalised surfaces. Kirschhöfer F1, Rieder A, Prechtl C, Kühl B, Sabljo K, Wöll C, Obst U, Brenner-Weiß G. Anal Chim Acta. 2013 Nov 13;802:95-102. doi: 10.1016/j.aca.2013.10.007. Epub 2013 Oct 22.
5. [5] Supported Lipid bilayers SLBs over various substrates [Nam-Joon Cho, Curtis W Frank, Bengt Kasemo & Fredrik Höök] Nature Protocols 5, - 1096 - 1106 (2010) doi:10.1038/nprot.2010.65
6. [6] G. Sauerbrey, Verwendung von Schwingquarzen zur Wägung dünner Schichten und Microwägung, Z. Phys. 155 (1959) 206–222.
7. [7] K.K. Kanazawa, J.G. Gordon II, The oscillation frequency of a quartz resonator in contact with a liquid, Anal. Chim. Acta 175 (1985) 99-105
8. [8] D. Wang, P. Mousavi, P.J. Hauser, W. Oxenham, C.S. Grant, Quartz crystal microbalance in elevated temperature viscous liquids: temperature effect compensation and lubricant degradation monitoring, Colloids and Surfaces A: Physicochemical and Engineering Aspects 268 (2005) 30–39.
9. [9] D. Johannsmann, Viscoelastic analysis of organic thin films on quartz resonators, Macromolecular Chemistry and Physics 200 (1999) 501-516.
10. [10] D. Johannsmann, Viscoelastic, mechanical, and dielectric measurements on complex samples with the quartz crystal microbalance, Physical Chemistry Chemical Physics 10 (2008) 4516–4534.
11. [11] D Johannsmann, K. Mathauer, G. Wegner, W. Knoll, Viscoelastic properties of thin films probed with a quartz-crystal resonator, Physical Review B 46 (1992) 7808–7815.
12. [12] R. Lucklum, C. Behling, P. Hauptmann, Thin film shear modulus determination with quartz crystal resonators, Sensors and Materials 11 (1999)
13. [13]Broadband spike excitation method for in-liquid QCM sensors, Pablo Resa, Pedro Castro, Jaime Rodríguez-López and Luis Elvira, Centro de Acústica Aplicada y Evaluación No Destructiva (CAEND), UPM-CSIC
14. [14] Electrical behaviour of AT-cut quartz crystal resonators as a function of overtone number M. Cassiède, J.H. Paillol, J. Pauly, J.-L. Daridon, Sensors and Actuators A 159 (2010) 174–183.
15. [15] G. Behling, R. Lucklum, P. Hauptmann, Fast three-step method for shear moduli calculation from quartz crystal resonator measurements, IEEE Transactions on Ultrasonics, Ferroelectrics, and Frequency Control 46 (1999) 1431–1438.
16. [16] D. Johannsmann, Derivation of the shear compliance of thin films on quartz resonators from comparison of the frequency shifts on different harmonics: a perturbation analysis, Journal of aplied Physics 89 (2001) 6356-6364
17. [17] Universidad de Benos Aires Facultad de Ciencias Exactas y Naturales, Aplicaciones analíticas de la balanza de cristal de cuarzo: microgravimetría y microrehología, Ernesto J. Calvo, Roberto Etchenique (1998)
18. [18] Extensions of the Ferry shear wave model for active linear and nonlinear microrheology, Sorin M. Mitran, M.Gregory Forest, Lingxing Yao, Brandon Lindley, David B. Hill, J. Non-Newtonian Fluid Mech. 154 (2008) 120–135
19. [19] J.D. Ferry, W.M. Sawyer, J.N. Ashworth, Behavior of concentrated polymer solutions under periodic stresses, J. Polym. Sci. 2 (1947) 593–611.
20. [20] van Dyke, Phys. Rev., 25, 895 (1925)
21. [21] Oppenheim: Señales y Sistemas, 2a. Ed.

LIST OF FIGURES

ANNEX

MATERIALS

 PC

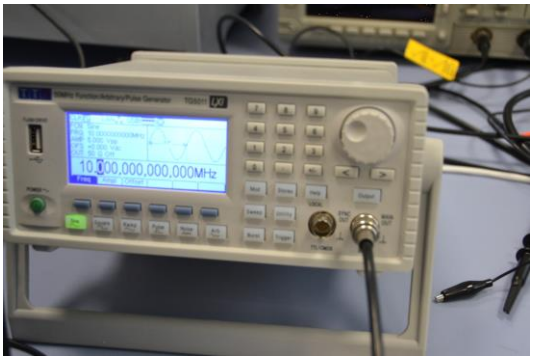 Function Generator

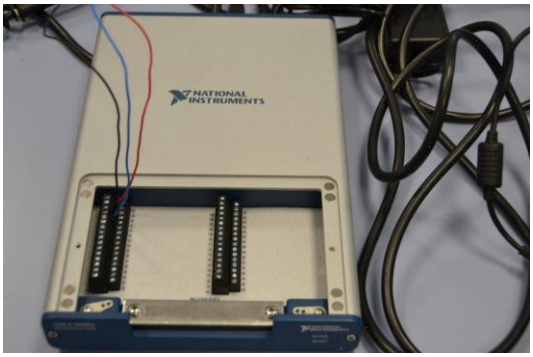 DAC

 Analog Oscilloscope

Digital Oscilloscope

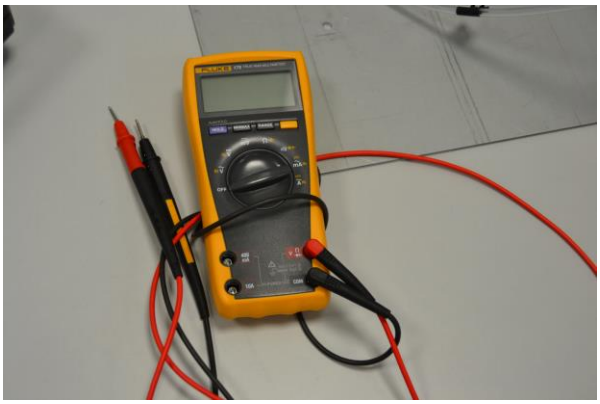
Multimetter


Welder + Sn + Cu connection board

DATA ACQUISITION PICTURES

It is shown the frequency shift indicated by the data acquisition system and the real frequency of the signal.

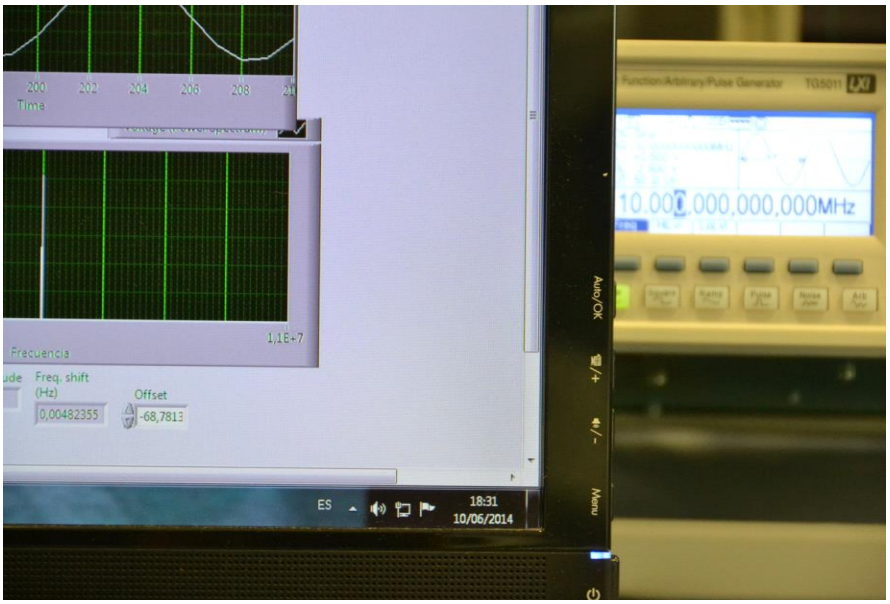

f=10MHz; fshift=0,00482355Hz

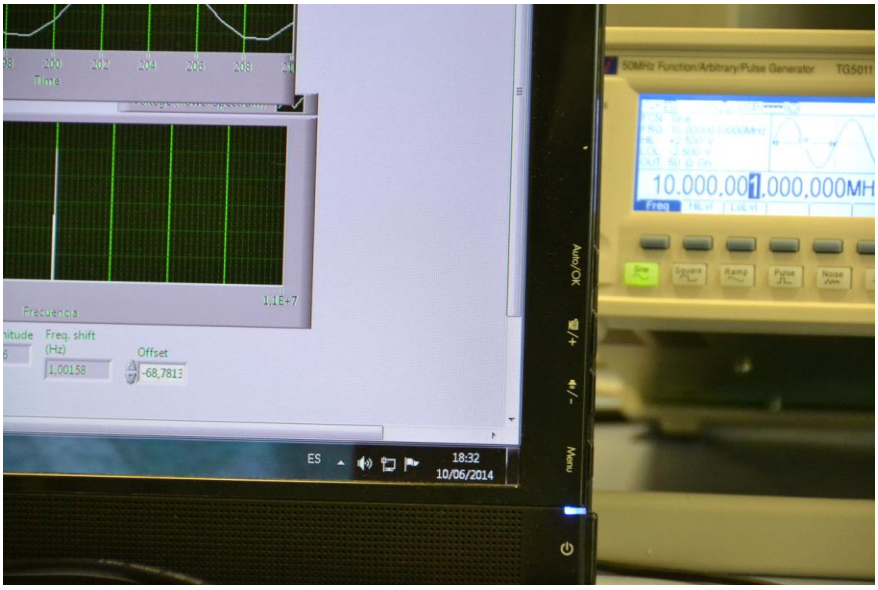

f=10,000001MHz; fshift=1,00158Hz

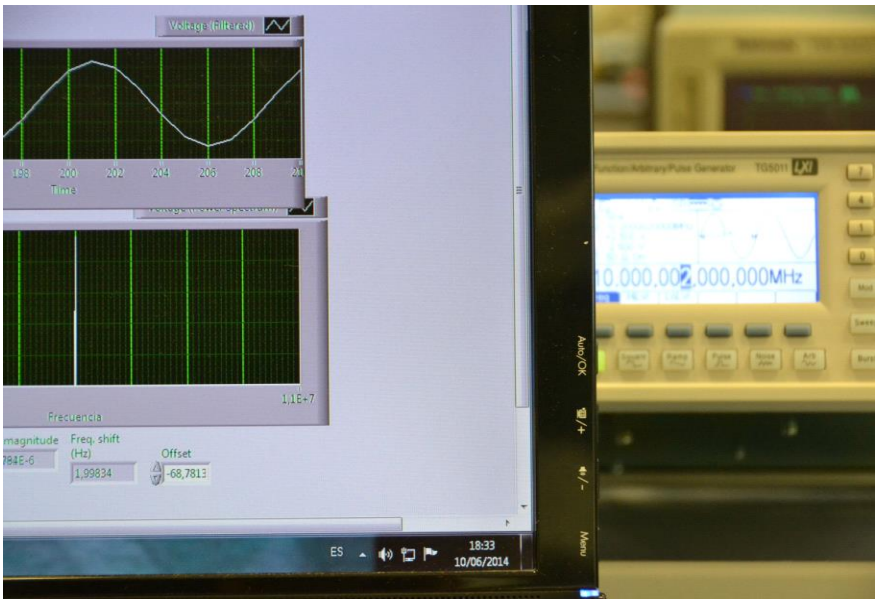

f=10,000002MHz; fshift=1,99834Hz

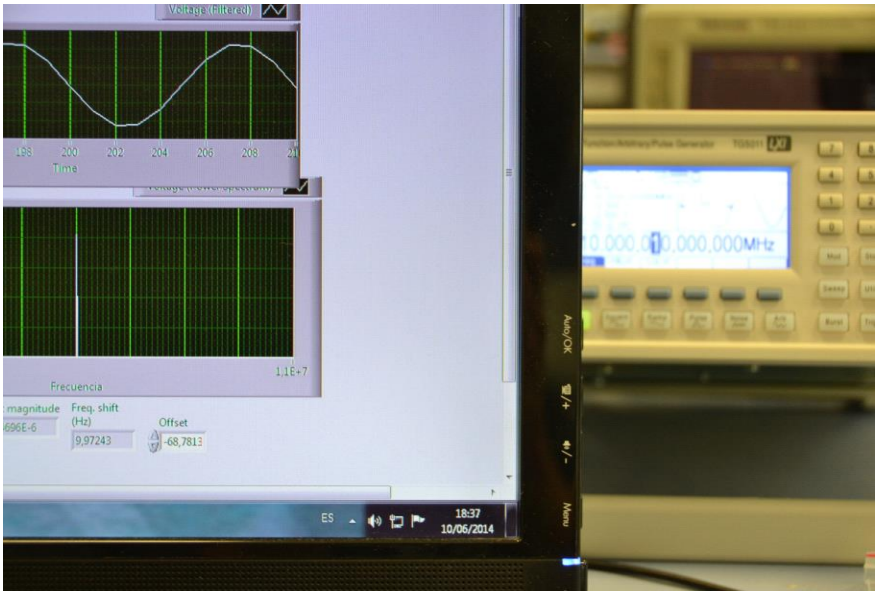

f=10,000010MHz; fshift=9,97243Hz

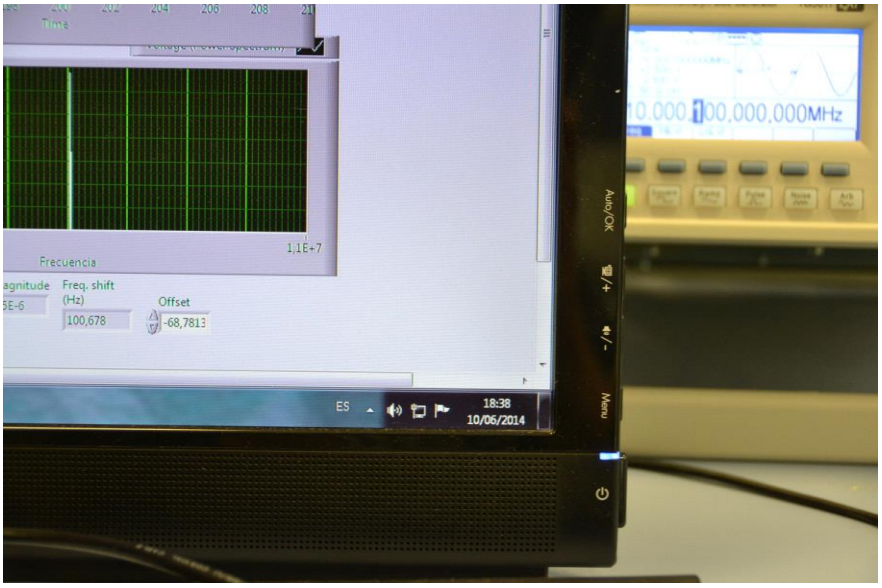

f=10,000100MHz; fshift=100,678Hz

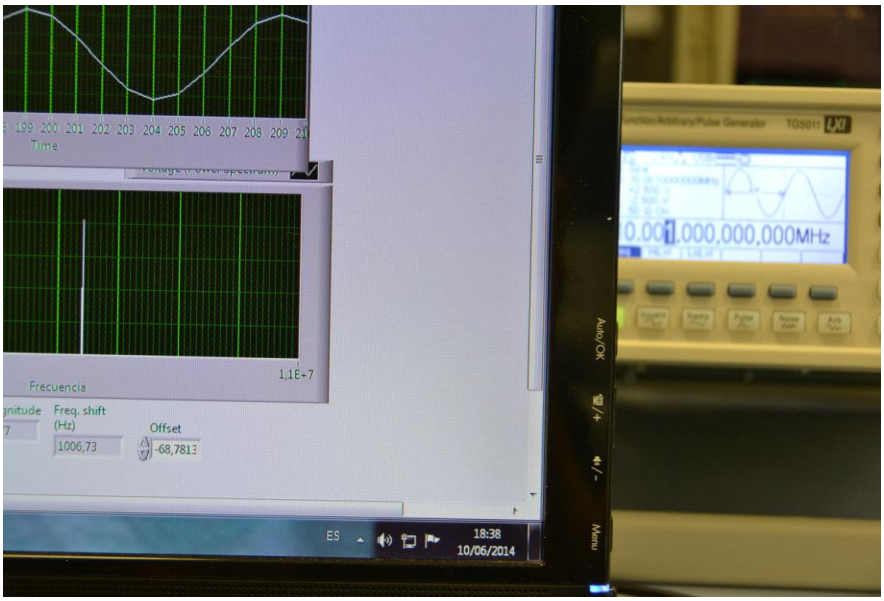

f=10,001000MHz; fshift=1006,76Hz